Microscopic description of the hot giant dipole resonance†

Nguyen Dinh Dang,[*1,*2] Kosai Tanabe,[*3] and Akito Arima[*4,*5]
[*1] *RI Beam Factory Project Office, RIKEN*
[*2] *Institute of Nuclear Science and Technique*
[*3] *Department of Physics, Saitama University*
[*4] *Ministry of Education, Science, Sports and Culture*
[*5] *Science and Technology Agency*

A systematic description of the evolution of the giant dipole resonance (GDR) at non-zero temperature T is presented within the Phonon Damping Model (PDM). The damping of the GDR is caused by coupling to all *ph*, *pp* and *hh* configurations at $T \neq 0$, where the coupling to *pp* and *hh* configurations is responsible for the increase and saturation of the GDR width as a function of T. The results of numerical calculations for the GDR width, the strength function and the integrated yield of the γ rays in ^{120}Sn and ^{208}Pb at $0 \leq T \leq 6$ MeV are obtained in a reasonable agreement with the most recent experimental data.

Introduction

First of all let me thank all of you for your participation in NUCOLEX 99. This is the strongest support that you have given to us in organizing this small scale symposium and workshop. NUCOLEX 99 is the best proof that the two topics: the nuclear incompressibility and the giant dipole resonance (GDR) built on compound states of highly excited nuclei (the hot GDR), that we choose to discuss at this meeting, are quite actual and of great importance. Indeed, I can say without exaggeration that the hot GDR is one of the phenomena that make the 50 year-old subject of giant resonance still very attractive.

The hot GDR has been studied intensively during the last two decades in heavy-ion fusion reactions (See Ref. 1 for the reviews). It has been now well established that the GDR width increases sharply with increasing excitation energy E^* up to $E^* \sim 130$ MeV in tin isotopes.[2–6] At higher E^* a saturation of the GDR width has been systematically reported.[7,8] Besides the width saturation the heavy-ion fusion measurements also showed that the integrated yield of the γ-rays from the decay of the hot GDR in tin isotopes seemed to saturate at $E^* \geq 350$ MeV in the GDR region within $12 \leq E_\gamma \leq 20$ MeV[9,10] and in the region above 20 MeV ($20 \leq E_\gamma \leq 35$ MeV).[10]

A considerable attention was attributed to the effects of angular momentum J and temperature T on the evolution of the hot GDR. Existing data and calculations showed that the angular momentum effects seemed to be unimportant at least for spins $J \leq 36\ \hbar$ and mass number $A \geq 120$.[5,7,11] Recently a new method employing small-angle light-ion scattering to excite the nucleus has been proposed to study the evolution of the GDR as a function of temperature T independently of angular momentum effects.[12,13] In particular, Ref. 13 has shown that the GDR widths measured in inelastic α-scattering experiments and in fusion reactions do not differ much in their evolution with T while the angular momentum is about 10 to 20 $\hbar$ lower in case of the inelastic scattering data. This is a clear indication that the effect of spin on the hot GDR in tin isotopes is not significant.

In the present situation an adequate approach to the damping of the hot GDR must give a consistent description of three following issues:
(1) the width increase and its saturation of the GDR as a function of T;
(2) the observed shape evolution of the GDR at various temperatures;
(3) the saturation of the integrated yield of γ rays at $E^* >$ 300 MeV in the GDR region and in the region above it.

Among the theoretical studies devoted to the damping of the hot GDR in recent years we refer two models, which have been proposed by the Milan group[14,15] and Catania group,[16–18] respectively. They have been frequently quoted by several experimental groups. Meanwhile, the authors of Ref. 19 have pointed out that not only the comparison of the calculated full width at half maximum (FWHM) with the experimental GDR width, but also the complete shape of the GDR strength function should be considered (issue (2)) to achieve a meaningful comparison between theory and experiment. The detailed analysis in Ref. 19, which includes the entire shape of the strength function, has shown that both the Milan model and the Catania model failed to reproduce the observed GDR shape.

In this talk we will present a review on a microscopic model for the damping of the hot GDR—the so-called Phonon Damping Model (PDM), which has been proposed and developed by us in Refs. 20 and 21. In the PDM the GDR is generated by a collective vibration (the GDR phonon), which is damped via coupling to all *ph* as well as *pp* and *hh* configurations appearing at $T \neq 0$. The novelty of the PDM is in the the coupling of the GDR phonon to particle-particle (*pp*) and hole-hole (*hh*) configurations, which is decisively impor-

† Keynote talk presented by Nguyen Dinh Dang at the RIKEN Symposium and Workshop on Selected Topics in Nuclear Collective Excitations (NUCOLEX 99), RIKEN, March 20–24, 1999

tant for a consistent description of the width increase and its saturation. The application of the PDM in a systematic study of the hot GDR width in ^{90}Zr, ^{120}Sn, and ^{208}Pb has been found in an overall agreement with the data in a wide temperature interval $0 \leq T \leq 6$ MeV, which covered both the regions of the width increase and its saturation. We also show in this talk how the PDM has been applied to a systematic description for the width and shape of the hot GDR in ^{120}Sn and ^{208}Pb. Finally, we hope that this study can shed a further light on the question under debate on whether the GDR disappears or still persists at high T.

Formalism

The PDM applies the double-time Green function method[22,23] to determine the physical processes which the GDR phonon undergoes and to derive a closed set of equations for the Green functions. The final goal is to obtain an approximate equation for the propagation of the GDR phonon, which is damped due to the presence of a polarization operator containing the effects of coupling to all ss' configurations ($(s,s') = (p,h), (p,p')$ and (h,h')). The damping of the GDR is defined as the imaginary part of the analytic continuation of the polarization operator in the complex energy plane. This is the advantage of using the double-time Green function method, since the usual Green function of the Schwinger type, in general, cannot be continued in the complex plane.

In this section we give the outline of two approximation schemes of the PDM. The first one (PDM-1) has been proposed and discussed in detail in Ref. 20. The PDM-1 treats the effects of higher-order graphs such as $1s1s'\otimes$phonon or/and two-phonon ones by selecting parameters of the model at $T = 0$. The second approximation scheme (PDM-2) is a further development to include explicitly all the forward-going processes up to two-phonon ones at $T \neq 0$ in the same order of the interaction strength. It has been discussed in detail in Ref. 21.

The PDM is based on a model Hamiltonian, which is composed of three terms, namely

$$H = \sum_s E_s a_s^\dagger a_s + \sum_q \omega_q Q_q^\dagger Q_q + \sum_{ss'q} F_{ss'}^{(q)} a_s^\dagger a_{s'} (Q_q^\dagger + Q_q). \quad (1)$$

The first term is the single-particle field, where $a_s^\dagger$ and a_s are creation and destruction operators of a particle or hole state with energy $E_s = \epsilon_s - \epsilon_F$ with ϵ_s being the single-particle energy and ϵ_F the Fermi energy. The second term is the phonon field, where $Q_q^\dagger$ and Q_q are the creation and destruction operators of a phonon with energy ω_q. The last term describes the coupling between the first two terms with $F_{ss'}^{(q)}$ denoting the coupling matrix elements. The indices s and s' denote particle (p, $E_p > 0$) or hole (h, $E_h < 0$), while the index q is reserved for the phonon state $q = \{\lambda, i\}$ with multipolarity λ (the projection μ of λ in the phonon index is omitted for simplicity). The sums over q run over $\lambda \geq 1$.

The PDM-1

The PDM-1 considers the following double-time Green functions, which describe[23]

(1) The propagation of a free particle (or hole):

$$G_{s';s}(t-t') = \langle\langle a_{s'}(t); a_s^\dagger(t')\rangle\rangle, \quad (2)$$

(2) The propagation of a free phonon:

$$G_{q';q}(t-t') = \langle\langle Q_{q'}(t); Q_q^\dagger(t')\rangle\rangle, \quad (3)$$

(3) The particle-phonon coupling in the single-particle field:

$$\Gamma^-_{s'q;s}(t-t') = \langle\langle a_{s'}(t)Q_q(t); a_s^\dagger(t')\rangle\rangle, \quad (4)$$
$$\Gamma^+_{s'q;s}(t-t') = \langle\langle a_{s'}(t)Q_q^\dagger(t); a_s^\dagger(t')\rangle\rangle, \quad (5)$$

(4) The transition between a nucleon pair and a phonon:

$$\mathcal{G}^-_{ss';q}(t-t') = \langle\langle a_s^\dagger(t)a_{s'}(t); Q_q^\dagger(t')\rangle\rangle. \quad (6)$$

A closed set coupled equations for Green functions in Eqs. (2)–(6) has been obtained in Ref. 20, following the standard method of double-time Green functions[23] applied to the Hamiltonian in Eq. (1). After making the Fourier transform to the energy plane E and eliminating functions $\Gamma^-(E)$, $\Gamma^+(E)$ and $\mathcal{G}(E)$ by expressing them in terms of $G_{s;s'}(E)$ and $G_{q;q'}(E)$, a set of two equations has been obtained for $G_{s;s'}(E)$ and $G_{q;q'}(E)$, which describe the p (h) and phonon propagations, respectively. For the propagation of a single p (or h) state $s = s'$ and a single phonon state $q = q'$ these equations become:

$$G_s(E) = \frac{1}{2\pi}\frac{1}{E - E_s - M_s(E)},$$
$$G_q^{(PDM1)}(E) = \frac{1}{2\pi}\frac{1}{E - \omega_q - P_q^{(PDM1)}(E)}, \quad (7)$$

where the mass operator $M_s(E)$ and the polarization operator $P_q^{(PDM1)}(E)$ are

$$M_s(E) = \sum_{q's'} F_{ss'}^{(q')} F_{s's}^{(q')} \left(\frac{\nu_{q'} + 1 - n_{s'}}{E - E_{s'} - \omega_{q'}} + \frac{n_{s'} + \nu_{q'}}{E - E_{s'} + \omega_{q'}}\right),$$
$$P_q^{(PDM1)}(E) = \sum_{ss'} F_{ss'}^{(q)} F_{s's}^{(q)} \frac{n_s - n_{s'}}{E - E_{s'} + E_s}. \quad (8)$$

The dampings of the single-particle state $\gamma_s(\omega)$ and of the phonon state $\gamma_q^{(PDM1)}(\omega)$ are derived as the imaginary parts of the analytic continuation in the complex energy plane $E = \omega \pm i\varepsilon$ of the mass $M_s(E)$ and polarization operators $P_q^{(PDM1)}(E)$, respectively:

$$\gamma_s(\omega) = \pi \sum_{q's'} F_{ss'}^{(q')} F_{s's}^{(q')} [(\nu_{q'} + 1 - n_{s'}) \times \delta(\omega - E_{s'} - \omega_{q'}) + (n_{s'} + \nu_{q'}) \times \delta(\omega - E_{s'} + \omega_{q'})], \quad (9)$$

$$\gamma_q^{(PDM1)}(\omega) = \pi \sum_{ss'} F_{ss'}^{(q)} F_{s's}^{(q)} (n_s - n_{s'}) \times \delta(\omega - E_{s'} + E_s). \quad (10)$$

The single-particle occupation number n_s (for phonon ν_q) in Eqs. (8) and (9) has the form of a Fermi (Bose) distribution folded with a distribution of Breit-Wigner type with an ω-dependent width $2\gamma_s(\omega)$ ($2\gamma_q(\omega)$) and centered at: $\tilde{E}_s = E_s + M_s(\tilde{E}_s)$ ($\tilde{\omega}_q = \omega_q + P_q^{(PDM1)}(\tilde{\omega_q})$). If γ_s is small, n_s can be well approximated by an exact Fermi distribution function with energy $\tilde{E}_s$. For ν_q this is not valid because γ_q can be large.

The main approximation of the PDM-1 consists of closing the hierarchy of the Green functions to Eqs. (2)–(6) based on the following decoupling approximation, which is originated from the approximate second quantization [22] and modified thermodynamically for the nonzero temperature case:

$$\langle\langle a_{s_1} \underbrace{Q_q^\dagger Q_{q'}}; a_s^\dagger \rangle\rangle = \delta_{qq'} \nu_q G_{s_1;s},$$
$$\langle\langle a_{s_1} \underbrace{Q_{q'} Q_q^\dagger}; a_s^\dagger \rangle\rangle = \delta_{qq'} (1 + \nu_q) G_{s_1;s}, \quad (11)$$
$$\langle\langle \underbrace{a_s^\dagger a_{s1}} (Q_{q'}^\dagger + Q_{q'}); Q_q^\dagger \rangle\rangle = \delta_{ss_1} n_s G_{q';q},$$
$$\langle\langle \underbrace{a_{s'} a_{s1}^\dagger} a_{s_1}; a_s^\dagger \rangle\rangle = \delta_{s's_1} (1 - n_{s'}) G_{s_1';s}. \quad (12)$$

This restricts the couplings in the mass operator $M_s(E)$ to at most $2p1h$ configurations if the phonon operator generates the collective ph excitation. The contribution of the coupling to higher-order Green functions of "$1p1h\oplus$phonon" or two-phonon type which causes the quantal (spreading) width Γ_Q of the ground-state (g.s.) GDR is assumed to be independent of T and included effectively by selecting the parameters of the model at $T = 0$. The justification of this approximation comes from the fact that the quantal width Γ_Q depends weakly on T as has been shown by several numerical calculations in Refs. 24 and 25 and will be confirmed in the PDM-2 version of our model below.

The PDM-2

The PDM-2 includes explicitly the coupling to all forward-going processes up to two-phonon ones by introducing in addition to the Green functions in Eqs. (2)–(6) the following double-time Green functions which describe

(5) The transition between a $1p1h\otimes$phonon ($1p1p\otimes$phonon or $1h1h\otimes$phonon) configuration and a phonon:

$$\Gamma_{ss'q';q}^{-;+}(t - t') = \langle\langle a_s^\dagger(t) a_{s'}(t) Q_{q'}(t); Q_q^\dagger(t') \rangle\rangle, \quad (13)$$

(6) The transition between two- and one-phonon configurations:

$$G_{q_1 q_2}^{--;+}(t - t') = \langle\langle Q_{q_1}(t) Q_{q_2}(t); Q_q^\dagger(t') \rangle\rangle. \quad (14)$$

The backward-going processes described by the Green functions $G_{q';q}^{+;+}(t - t') = \langle\langle Q_{q'}^\dagger(t); Q_q^\dagger(t') \rangle\rangle$, $\Gamma_{ss'q';q}^{+;+}(t - t') = \langle\langle a_s^\dagger(t) a_{s'}^\dagger(t) Q_{q'}^\dagger(t); Q_q^\dagger(t') \rangle\rangle$, and $G_{q_1 q_2}^{++;+}(t - t') = \langle\langle Q_{q_1}^\dagger(t) Q_{q_2}^\dagger(t); Q_q^\dagger(t') \rangle\rangle$ are neglected because the poles of their Fourier transforms would be located at negative energies faraway from the GDR region. Hence, just like the Y-amplitudes in the random-phase approximation (RPA), they are not expected to affect noticeably the damping of GDR.

A set of coupled equations for an hierarchy of Green functions has been derived applying again the standard procedure described in Ref. 23. Employing the decoupling scheme similar to Eqs. (11) and (12) we closed this set to the functions (2)–(6), (13) and (14). Making then the Fourier transform to the energy plane E and performing several simple manipulations to express the Fourier transforms of other functions in the set in terms of the Fourier transform of function (3) by using the same decoupling scheme, we come to the final expression for the propagation of a single phonon ($q = q'$) as

$$G_q^{(PDM2)}(E) = \frac{1}{2\pi} \frac{1}{E - \omega_q - P_q^{(PDM2)}(E)}. \quad (15)$$

The explicit form of the polarization operator $P_q^{(PDM2)}(E)$ in Eq. (15) is

$$P_q^{(PDM2)}(E) = \sum_{ss's_1q'} \frac{F_{ss'}^{(q)}}{E - E_{s'} + E_s} \times \Big[\frac{F_{s's_1}^{(q')} \mathcal{M}_{ss_1}^{qq'}(E)}{E - E_{s_1} + E_s - \omega_{q'}} - \frac{F_{s_1 s}^{(q')} \mathcal{M}_{s_1 s'}^{qq'}(E)}{E - E_{s'} + E_{s_1} - \omega_{q'}} \Big], \quad (16)$$

where the vertex function $\mathcal{M}_{ss'}$ is

$$\mathcal{M}_{ss'}^{qq'}(E) = \sum_{s_2} \Big\{ \frac{(1 - n_{s'} + \nu_{q'})(n_s - n_{s_2})}{E - E_{s_2} + E_s} F_{s's_2}^{(q')} F_{s_2 s}^{(q)} - \frac{(n_s + \nu_{q'})(n_{s_2} - n_{s'})}{E - E_{s'} + E_{s_2}} F_{s_2 s}^{(q')} F_{s's_2}^{(q)} + n_{s_2}(n_s - n_{s'}) \Big[\frac{F_{s's}^{(q)} F_{s_2 s_2}^{(q')}}{E - \omega_q - \omega_{q'}} + \delta_{qq'} \sum_{q_1} \frac{F_{s's}^{(q_1)} F_{s_2 s_2}^{(q_1)}}{E - \omega_{q_1} - \omega_{q'}} \Big] \Big\}. \quad (17)$$

The phonon damping $\gamma_q^{(PDM2)}(\omega)$ is again defined as the analytic continuation of the polarization operator $P_q^{(PDM2)}(E)$ in Eq. (16) into the complex energy plane, namely

$$\gamma_q^{(PDM2)}(\omega) = |\mathrm{Im} P_q^{(PDM2)}(\omega \pm i\varepsilon)|. \quad (18)$$

Function $P_q^{(PDM2)}(E)$ in Eq. (16) includes all $1s1s'$, $1s1s' \otimes$ phonon ($(s, s') = (p, h), (p, p')$ and (h, h')) and two-phonon processes at the same second order in $F_{ss'}^{(q)}$. In the limit of high temperature the vertex function $\mathcal{M}_{ss'}^{qq'}$ in Eqs. (16) and (17) tends to

$$\mathcal{M}_{ss'}^{q_1 q'}(E)|_{T\to\infty} \longrightarrow \frac{1}{4} \sum_{s_2} \Big\{ \frac{1}{\omega_{q'}} \Big[\frac{E_{s_2} - E_s}{E - E_{s_2} + E_s} F_{s's_2}^{(q')} F_{s_2 s}^{(q)} + \frac{E_{s_2} - E_{s'}}{E - E_{s'} + E_{s_2}} F_{s_2 s}^{(q')} F_{s's_2}^{(q)} \Big] + \frac{1}{2T}(E_{s'} - E_s) \Big[\frac{F_{s's}^{(q)} F_{s_2 s_2}^{(q')}}{E - \omega_q - \omega_{q'}} + \delta_{qq'} \sum_{q_1} \frac{F_{s's}^{(q_1)} F_{s_2 s_2}^{(q_1)}}{E - \omega_{q_1} - \omega_{q'}} \Big] \Big\}, \quad (19)$$

which means that it decreases as $O(T^{-1})$ with increasing T because of the factor T^{-1} in front of two-phonon terms on the r.h.s. of Eq. (19). Neglecting these two-phonon processes would lead to a constant width at high temperature because the first two terms on the r.h.s. of Eq. (19) are independent of T provided $F^{(q)}_{ss'}$, E_s and ω_q do not or depend weakly on T. More details on the derivation of the PDM-2 equations and their diagrammatic illustration in connection with the NFT[24] can be found in Ref. 21.

In both versions of the PDM, the mechanism that determines the behavior of the GDR as a function of temperature is the coupling of GDR to both *ph* as well as *pp* and *hh* configurations. This lies mathematically in the factor $n_s - n_{s'}$ in Eqs. (8), (10) and (17). In order to demonstrate this effect, we display in the top pannels of Fig. 1 the single particle occupation number n_s as a function of temperature for $s = p$ and h. Both the occupation numbers n_h and n_p approach $\frac{1}{2}$ at $T \to \infty$, but from different sides. As a result, the difference $n_h - n_p$ decreases with increasing T (Fig. 1 bottom left). As we will see later, this leads to the decrease of the quantal width as the temperature increases. On the contrary, the difference $n_h - n_{h'}$ $(n_p - n_{p'})$ increases with increasing T in the low temperature region, but after reaching the maximum, it decreases at high T (Fig. 1 bottom right). This leads to the increases of the thermal width in the low temperature region, and its saturation in the region where the difference $n_h - n_{h'}$ $(n_p - n_{p'})$ reaches the maximum. The PDM just gives a natural and simple explanation of the temperature dependence of the GDR full width in the whole temperature interval $0 \leq T \leq$ 5–6 MeV.

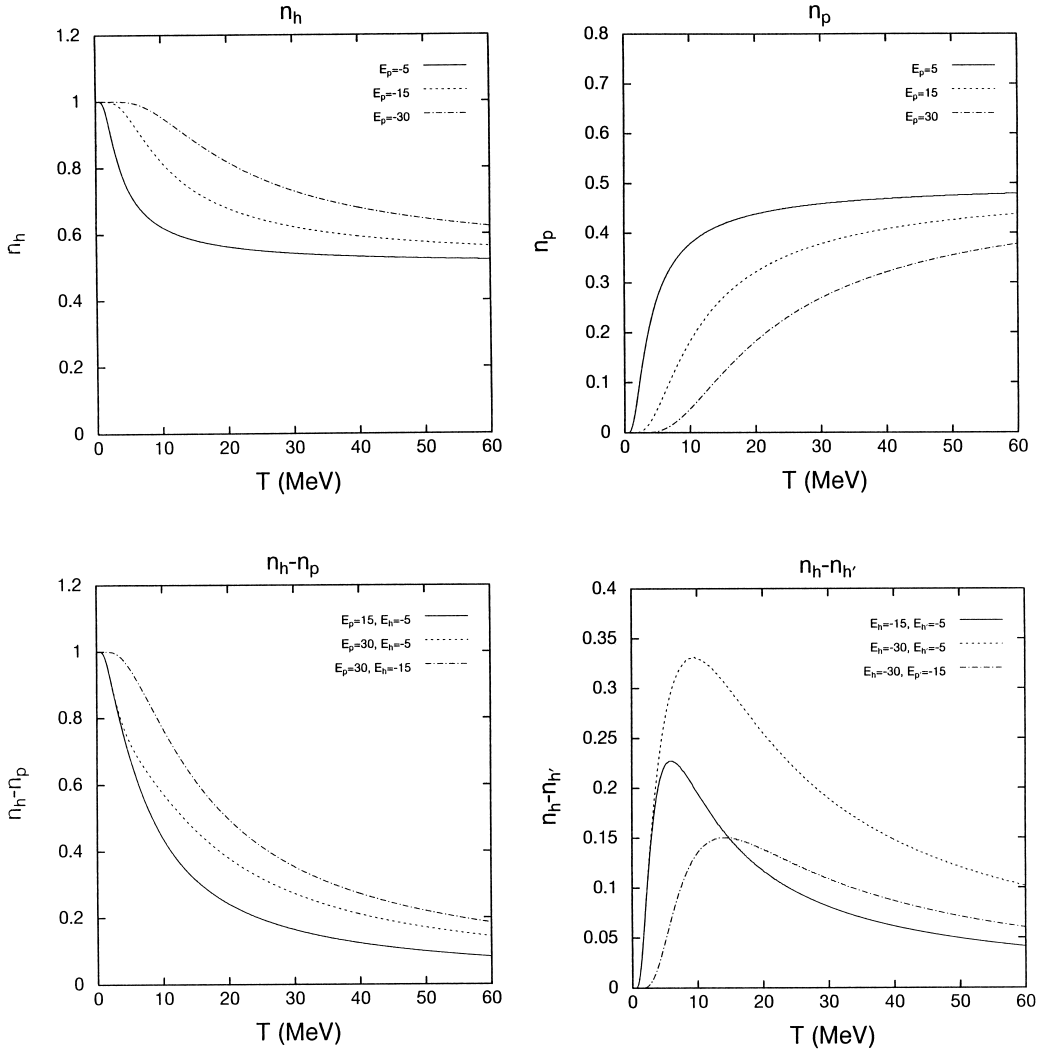

Fig. 1. Single particle occupation number as a function of temperature.

GDR parameters and integrated yield of γ rays

The GDR energy ω_{GDR} is determined within the PDM at the pole $\bar{\omega}$ of $G^{(i)}_q(\omega)$, i.e.

$$\bar{\omega} - \omega_q - P^{(i)}_q(\bar{\omega}) = 0, \tag{20}$$

where $\bar{\omega}$ is real and $P^{(i)}_q(\bar{\omega})$ is the real part of $P^{(i)}_q(E)$ with $P^{(i)}_q(E)$ being defined from Eq. (8) (i = PDM1) or Eq. (16) (i = PDM2).

The FWHM Γ_{GDR} of the GDR at energy ω_{GDR} is defined twice as much as the phonon damping $\gamma^{(i)}_q(\omega)$

$$\Gamma^{(i)}_{GDR} = 2\gamma^{(i)}_q(\omega = \bar{\omega}). \quad (21)$$

The shape of the GDR is described by the strength function $S^{(i)}_q(\omega)$, which is derived from the spectral intensity $J^{(i)}_q(\omega)$ in the standard way using the analytic continuation of the Green function $G^{(i)}_q(\omega \pm i\varepsilon)$ [22] and by expanding $P^{(i)}_q(\omega)$ around $\bar{\omega}$[23]. The final form of $S^{(i)}_q(\omega)$ is

$$S^{(i)}_q(\omega) = \frac{1}{\pi} \frac{\gamma^{(i)}_q(\omega)}{(\omega - \bar{\omega})^2 + [\gamma^{(i)}_q(\omega)]^2}. \quad (22)$$

Since the damping $\gamma^{(i)}_q(\omega)$ depends on the energy variable ω, which runs over the γ-ray energy E_γ, the shape of the strength function $S^{(i)}_q(\omega)$, strictly speaking, is not given by a single Breit-Wigner curve. The spectral intensity $J^{(i)}_q(\omega)$ is related to the strength function $S^{(i)}_q(\omega)$ as

$$J^{(i)}_q(\omega) = \frac{S^{(i)}_q(\omega)}{e^{\omega/T} - 1}. \quad (23)$$

This form is proportional to the exponential shape of the γ-ray spectra observed in experiments while the strength function $S^{(i)}_q(\omega)$ can be directly compared with the divided spectra in the linear scale normalized by a strength constant.

The value of the FWHM of the GDR $\Gamma^{(i)}_{GDR}$ given by Eq. (21) is more reliable than the width extracted from the energy dispersion

$$\sigma = \sqrt{(\overline{E^2}) - (\overline{E})^2}, \quad (24)$$

$$\overline{E^k} = \frac{\int_{E_1}^{E_2} \omega^k S_q(\omega) d\omega}{\int_{E_1}^{E_2} S_q(\omega) d\omega}, \quad (k = 1, 2), \quad (25)$$

because the variance σ is sensitive to the choice of cutoff energies E_1 and E_2 introduced in the distant wings of the strength distribution, especially when the strength function is described by a Lorentzian or a Breit-Wigner curve. Meanwhile the empirical widths are the FWHM, which can be described by Γ_{GDR} in Eq. (21).

The present formalism considers the hot GDR, its width and shape as a result of averaging over the grand canonical ensemble at a given temperature. Therefore the yield of the γ-ray can be calculated here following the standard statistical model using simplifying assumptions. They include a T^2-dependence for the neutron-decay width and the first order of the logarithmic expansion of the level density.[26] This allows us to calculate the integrated yield $Y^{(i)}_\gamma$ within the interval $E_1 \le \omega \le E_2$ as follows:

$$Y^{(i)}_\gamma \propto \frac{1}{T^2} \int_{E_1}^{E_2} \omega^3 J^{(i)}_q(\omega) e^{(B_n/T)} d\omega, \quad (26)$$

where B_n represents the neutron binding energy and $J_q(\omega)$ is the spectral intensity defined in Eq. (23). This quantity should be compared with the empirically extracted yield, where a Lorentzian strength function $f_{GDR}(\omega)$ multiplied by $\exp(-\omega/T)$ was used instead of $J^{(i)}_q(\omega)$.[1] We have checked that in the region of the GDR peak a Lorentzian distribution centered at ω_{GDR} with a FWHM Γ_{GDR} has almost the same shape as the Breit-Wigner one divided by ω_{GDR} with the same width.

Numerical results

Ingredients of numerical calculations

We assume that the GDR is generated by a single collective and structureless phonon with energy ω_q close to the energy ω_{GDR}. The single-particle energies defined in the Woods-Saxon potentials at $T = 0$ were used in calculations. The levels near the Fermi surface for ^{208}Pb are replaced with the empirical ones. The procedure of selecting ω_q and the matrix elements $F^{(q)}_{ss'}$ of the coupling to ph, pp and hh configurations is as follows.

In the PDM-1 the coupling matrix elements $F^{(q)}_{ss'}$ are parametrized as $F^{(q)}_{ph} = F_1$ for $(s, s') = (p, h)$ and $F^{(q)}_{pp'} = F^{(q)}_{hh'} = F_2$ for $(s, s') = (p, p')$ or (h, h').

In general the PDM-2 contains the explicit coupling to phonons with different multipolarities λ. In the present application of the PDM-2, as a test for the effect of coupling to quadrupole vibration we retain only dipole and quadrupole phonons in the two-phonon configuration mixing. Consequently, from the sums on the r. h. s. of Eqs. (16) and (17) there remain only one dipole phonon with $q = q'$, which corresponds to the GDR ($\lambda = 1$) and one quadrupole phonon with q_1 with energy close to the energy $E_{2^+_1}$ of the first quadrupole state ($\lambda = 2$). The values of ω_q and F_1 (within PDM-1) or $F^{(1)}_1$ (within PDM-2) have been selected so that the solution $\bar{\omega}$ of Eq. (20) is equal to the empirical value of ω_{GDR} while $\Gamma_{GDR}(\bar{\omega})$ reproduces the empirical FWHM of the g.s. GDR (i.e. the quantal width Γ_Q at $T = 0$). The value of F_2 (for PDM-1) or $F^{(1)}_2$ (for PDM-2) has been chosen so that the energy $\bar{\omega}$ is stable against varying T. In PDM-2 we first set the ratio $r = F^{(2)}_i / F^{(1)}_i$ ($i = 1, 2$) when choosing ω_q, $F^{(1)}_1$ and $F^{(2)}_1$ in order to achieve a stable solution for Eq. (20). These parameters are kept unchanged when T is varied. This ensures that all the T-dependence comes from dynamical effects of configuration mixing, and not due to adjusting parameters. The smearing parameter ε in Eq. (18) was chosen to be 0.5 MeV. The results were found to be stable against varying ε within $0.2 \le \varepsilon \le 1.0$ MeV. The dipole sum rule was also checked to be conserved against varying T. The PDM-1 parameters ω_q, F_1 and F_2 (three parameters) have been given in Ref. 20. The selected values of the PDM-2 parameters ω_q, $F^{(1)}_1$, $F^{(1)}_2$ and r (four parameters) for ^{120}Sn and ^{208}Pb are presented in Ref. 21.

Temperature dependence of GDR width

The GDR widths Γ_{GDR} calculated within two versions of the PDM are shown in Fig. 2 (a) for ^{120}Sn and in Fig. 2 (b) for ^{208}Pb. They are compared with the revised data from inelastic α-scattering experiments[13] and also from Refs. 7 and 8. The values of the width obtained within the PDM-1 (dotted and dashed curves) have been reported previously Ref. 20. It is seen that the theoretical curves in both versions of the PDM reproduce reasonably well the data including the width saturation at $T \ge$ 3–4 MeV in case of ^{120}Sn.[7,8] The values of the width obtained within the PDM-2 (solid and dash-dotted curves) are somewhat smaller than those calculated in PDM-1 at $T \ge$ 1.5–2 MeV in ^{120}Sn and $T \ge$ 0.7–0.8 MeV

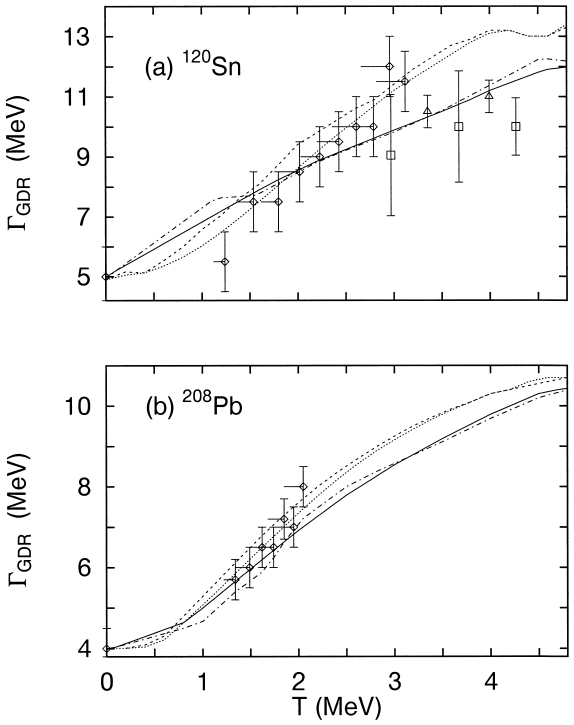

Fig. 2. Total width of GDR as a function of T for ^{120}Sn (a) and ^{208}Pb (b). Dotted: results within PDM-1 without the effect of single-particle damping. Dashed: results within PDM-2 including the effect of single-particle damping. Solid: results within PDM-2 without the effect of single-particle damping. Dash-dotted: results within PDM-2 including the effect of single-particle damping. Squares, triangles and diamonds: data from Refs. 7, 8 and 13, respectively.

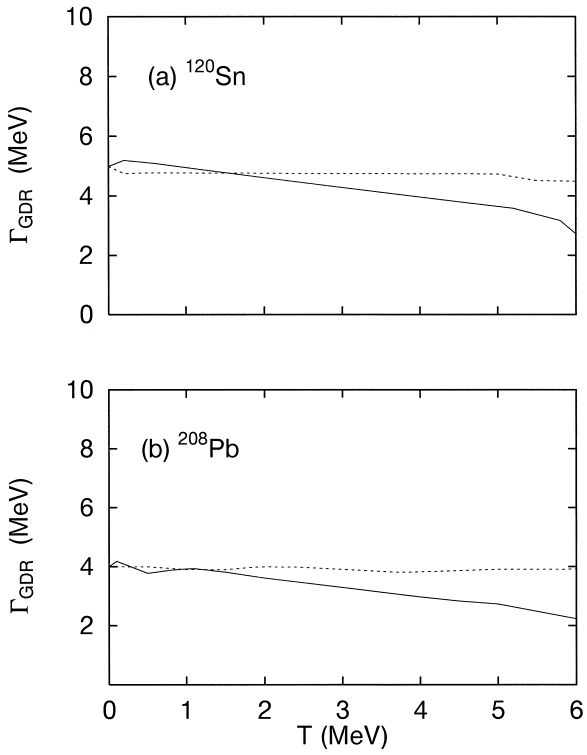

Fig. 3. Quantal width $\mathbf{\Gamma}_Q$ as a function of T for ^{120}Sn (a) and ^{208}Pb (b). Solid: quantal width $\mathbf{\Gamma}_Q$ obtained within PDM-2. Dashed: quantal width $\mathbf{\Gamma}_Q$ obtained within PDM-2 when the contribution of the two-phonon processes at $T \neq 0$ is omitted.

in ^{208}Pb. The reason is that in the PDM-1 the coupling to all multipolarities is included effectively in a sense of average, while in the PDM-2 the present calculation includes only one dipole phonon and one quadrupole phonon in the doorways. On the other hand the slight difference between the results obtained in two approximations indicates the importance of mixings with $\lambda = 1$ and 2 in reproducing the hot GDR width and shape as will be seen later. The effect of the single-particle damping on the GDR width is seen to be week in both versions of the PDM by comparing the solid curve obtained without this effect with the dash-dotted curve calculated with taking into account this effect in PDM-2. Similarly, one should compare the dotted and dashed curves for PDM-1.

It has been shown in PDM-1[20] that the total width is composed of the quantal width Γ_Q due to coupling of the GDR phonon to ph configurations and the thermal width Γ_T due to coupling to pp and hh configurations at $T \neq 0$. One of the main conclusions of Ref. 20 was that the behavior of the total width at high temperatures is mostly driven by the thermal width Γ_T since the quantal width Γ_Q decreases slightly as temperature increases. In order to see whether this conclusion still holds within the PDM-2 which includes higher-order processes up to two-phonon ones we have performed the calculations of Γ_Q by switching off the coupling to pp and hh configurations in the sums on the r.h.s. of Eqs. (16) and (17). The results are displayed in Fig. 3 by solid curves which show a clear decrease as T increases. Exclusion of two-phonon terms at $T \neq 0$ in Eq. (17) results in a quantal width, which is practically independent of T (dashed curves) similarly to the conclusion of Ref. 24.

The GDR widths obtained within PDM-1 for ^{120}Sn and ^{208}Pb in a larger temperature interval up to $T = 6$ MeV are shown in Fig. 4 (a) and (b), respectively . The results are compared with the inelastic α-scattering data from Ref. 12. The theoretical curves for the full width show a clear saturation at $T \geq 4$ MeV. At this symposium, Snover reported on the new data analysis and measurements that seem to have no evidence of the width saturation up to $T \simeq 3.2$ MeV. According to our calculations discussed above, the temperature region below $T = 3.2$ MeV is the region where the GDR width is still expected to increase.

Evolution of GDR shape

The GDR strength function $S_q^{(PDM1)}(\omega)$ calculated within the PDM-1 is compared with the normalized experimental one $f_{E1}(E_\gamma)$[13] in Fig. 5 for ^{120}Sn and Fig. 6 for ^{208}Pb. The experimental values of E_γ have been shifted up by 1.5 MeV in ^{120}Sn and by 1 MeV in ^{208}Pb in order to achieve a best agreement. This is due to the fact that the PDM assumes a temperature-independent GDR energy ω_{GDR} equal to the energy of the g.s. GDR. The solution $\bar{\omega}$ of Eq. (20) has been found to be stable around 15.4 MeV for ^{120}Sn and 13.5 MeV for ^{208}Pb at all temperatures using the selected values of the parameters in both versions PDM-1 and PDM-2. Meanwhile the experimental resonance energy was found in Ref. 13 to be lower than the g.s. GDR energy by an amount roughly equal to this shift. In other measurements the g.s. GDR energy ($T = 0$) has been used for the best fit of the data at $T \neq 0$.[2,4–9] At present no systematic dependence of the GDR energy on the excitation energy E^* (or temperature

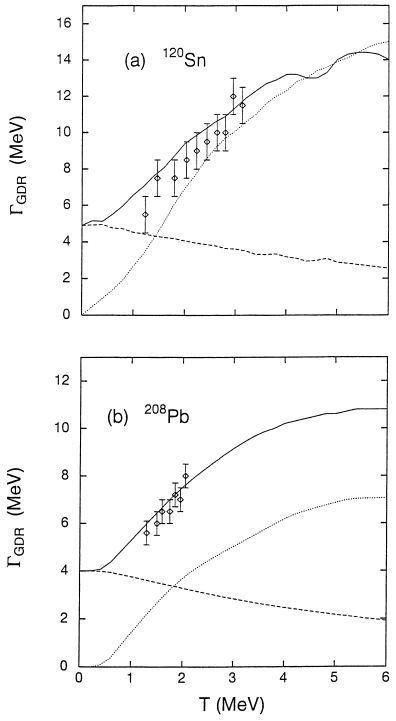

Fig. 4. Total width of GDR obtained within PDM-1 as a function of T for ^{120}Sn (a) and ^{208}Pb (b). Dashed: quantal width. Dotted: thermal width. Solid: full width. Date are from Ref. 12.

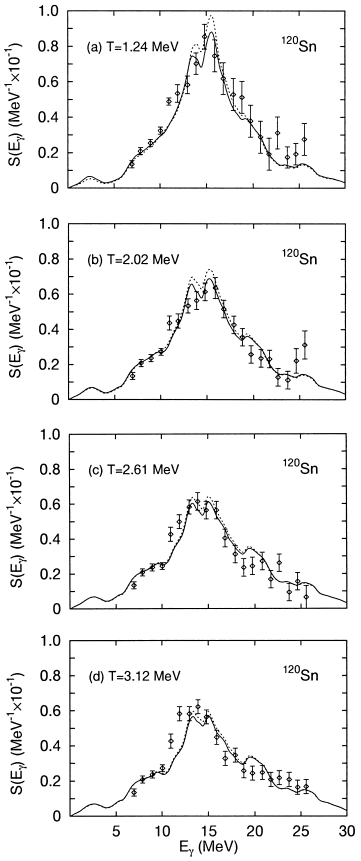

Fig. 5. GDR strength function in ^{120}Sn calculated within PDM-1 at several temperatures. Solid: results obtained with the effect of single-particle damping. Dashed: results without the effect of single-particle damping. Diamonds: normalized data from Ref. 13.

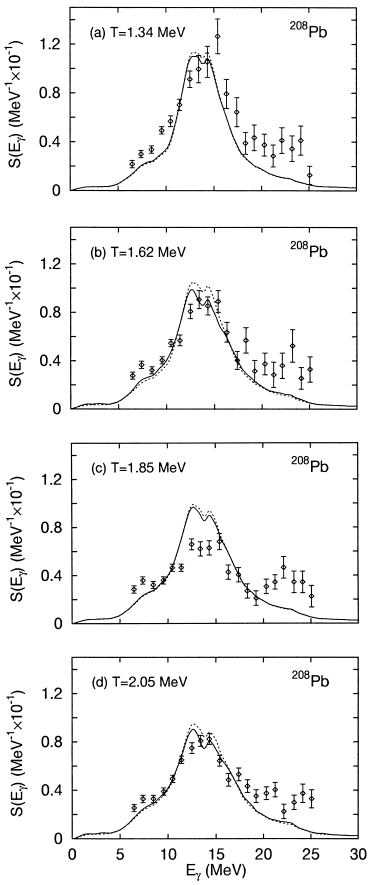

Fig. 6. Same as Fig. 5 for ^{208}Pb.

T) has been confirmed and more studies are called for to resolve this issue. Therefore we do not consider reasonable at this stage to vary the parameters of our model with temperature to achieve the decrease of the GDR energy in Ref. 13. Inclusion of this energy shift yields a good agreement between the calculations in PDM-1 and the available data for the evolution of the GDR shape in ^{120}Sn (Fig. 5). The PDM-1 could even reproduce the fine structure on two shoulders of the experimental resonance peak, especially the one in the low-energy region. For ^{208}Pb the data do not strictly follow a Breit-Wigner or Lorentzian shape. At $T = 1.85$ MeV the experimental shape of the GDR has even a pronounced structure between 20–25 MeV while the resonance peak seems to be too low. Nonetheless the agreement between the results of calculations in the PDM-1 and the data for ^{208}Pb is also satisfactory (Fig. 6).

Shown in the left columns ((a)-(d)) of Figs. 7 and 8 are the results of calculations within PDM-2 and the same data from Figs. 5 and 6. Since the present version of the PDM-2 restricts the coupling to *ph*, *pp* and *hh* configurations via the doorways, which included only dipole and quadrupole phonons, the calculated shape is found slightly narrower and higher at its peak position. This restriction also causes some structure between (15–20) MeV at energies around $\omega_q + \omega_{q_1}$.

Nonetheless an overall agreement between theory and data is achieved also in PDM-2. Taking into account more collective quadrupole phonons or/and phonons of higher multipolarities can improve the agreement. However it would certainly make

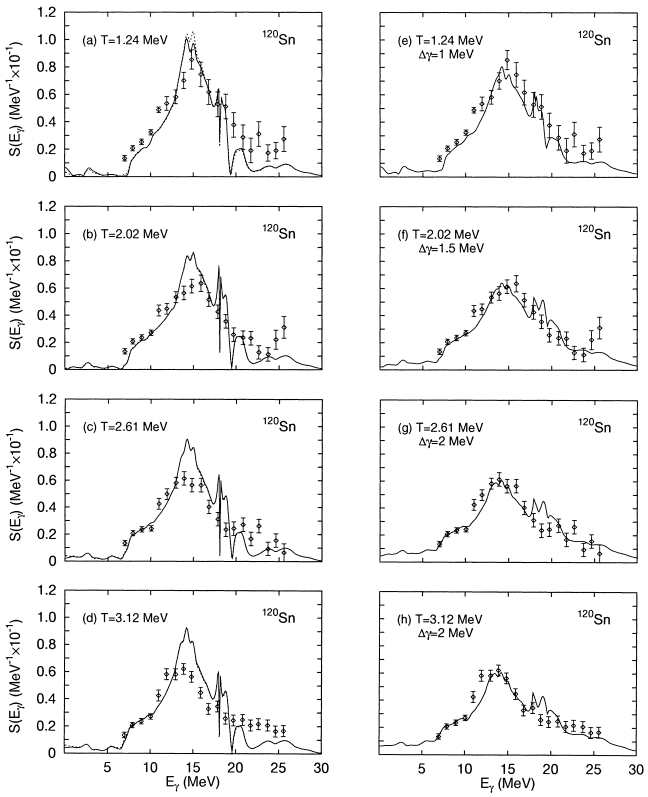

Fig. 7. GDR strength function in ^{120}Sn calculated within PDM-2 at several temperatures. Notation is the same as in Fig. 3. In (e) - (f): results of calculations using $\gamma_q^{(PDM2)}(\omega)+\Delta\gamma$ instead of $\gamma_q^{(PDM2)}(\omega)$ are shown with the corresponding values of $\Delta\gamma$.

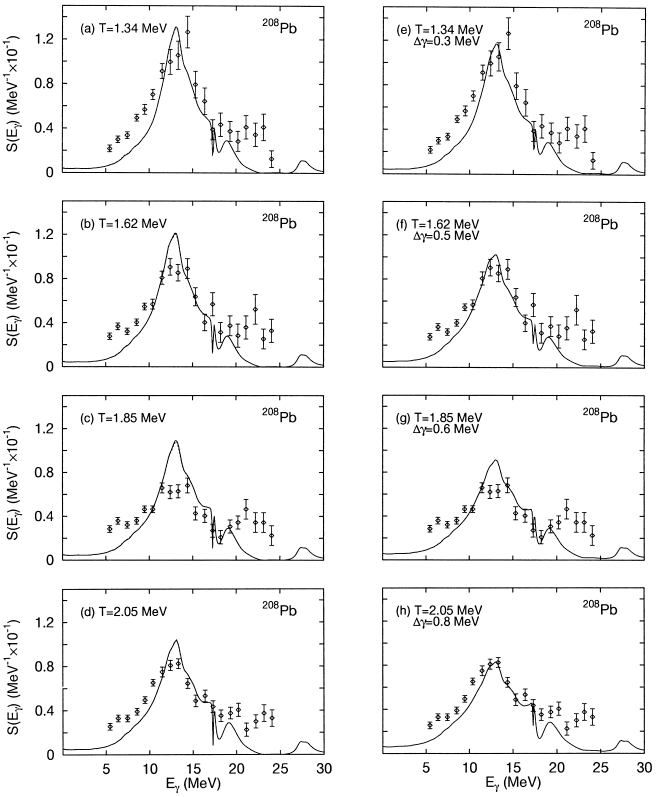

Fig. 8. Same as Fig. 7 for ^{208}Pb.

the calculations within the PDM-2 more complicate. At least it would increase the number of the parameters of the model unless the structure of phonon operators is defined microscopically in terms of *ph* pairs as in the RPA. In the meantime a simple way to include effectively the contribution of the missing doorway configurations in the present calculations within the PDM-2 is to add a parameter $\Delta\gamma$ to $\gamma_q^{(PDM2)}(\omega)$ to minimize the discrepancy between $\Gamma_{GDR}^{(PDM2)}$ and $\Gamma_{GDR}^{(PDM1)}$. The strength functions calculated with increasing $\gamma_q^{(PDM2)}(\omega)$ by $\Delta\gamma$ are shown in the right columns ((e)-(h)) of Figs. 7 and 8. The overall agreement between theory and experiment is clearly improved. In our opinion it is unlikely that the main features of the results obtained within PDM-1 or PDM-2 (with this additional parameter $\Delta\gamma$) will be altered significantly by more sophisticated microscopic calculations, given the fact that the hot GDR occurs in the stochastization region of high level densities and high excitation energies.[27)]

This comparison also shows that, despite its simplicity, the PDM-1 has offered a quite reasonable agreement with the data for the width and shape of the hot GDR. The PDM-2 on the other hand has demonstrated that including explicitly the coupling to higher-order configurations does not change the conclusions of the PDM-1, in particular regarding the weak temperature dependence of the quantal width Γ_Q. This is a clear indication that the quantal effect of complex configurations mixing is relatively insensitive to the change of temperature. Therefore it can be well incorporated in the parameters of the model selected at $T = 0$ as has been done in PDM-1. The evolution of the GDR shape at $T \neq 0$, therefore, does not depend much on the complexity of the doorway components, but is governed mostly by the presence of the coupling to incoherent *pp* and *hh* configurations.

Integrated yield of γ rays

The integrated yields $Y_\gamma^{(i)}$ of γ rays in ^{120}Sn calculated within PDM-1 and PDM-2 are plotted as a function of excitation energy E^* in Fig. 9 ((a) and (b)). The results have been obtained upon performing the integration in Eq. (25) within two intervals $12 \leq E_\gamma \leq 20$ MeV $+\Delta E_\gamma$ and 12 MeV $+\Delta E_\gamma \leq E_\gamma \leq 35$ MeV. Since the width calculated in PDM-1 is larger than the one obtained within PDM-2, the value of ΔE_γ has been chosen to be 1 MeV (dashed curve) and 2 MeV (dash-dotted curve) within PDM-1, and 0 (solid curve) within PDM-2. These results are compared with the data within (12–20) MeV[9,10)] (Fig. 9 (a)) and within (20–35) MeV [10)] (Fig. 9 (b)), respectively. The results reproduce reasonably well the observed saturation of the yield in the GDR region. In the region (20–35) MeV (Fig. 9 (b)) the PDM-1 gives somewhat larger values for the integrated yield (dashed and dash-dotted curves) as compared to the data while the results obtained within the PDM-2 (solid curve) are found in a better agreement with the data. In general the trend of saturation of the yield is also reproduced by the PDM in this region. The saturation of the yield at $E^* \geq 300$ MeV is understood here as a natural consequence of the saturation of the GDR shape and its width at $T > 4$ MeV, not by an exceedingly large value of the width as has been proposed previously in Refs. 9, 16–18. It is worth noticing that the value of the integrated yield in the region above the GDR (within (20–35) MeV) is more sensitive to the change in the value of ΔE_γ than within the GDR region (12–20) MeV. The reason is that the integration in Eq. (25) involved larger energies in the region above the GDR and also that the dis-

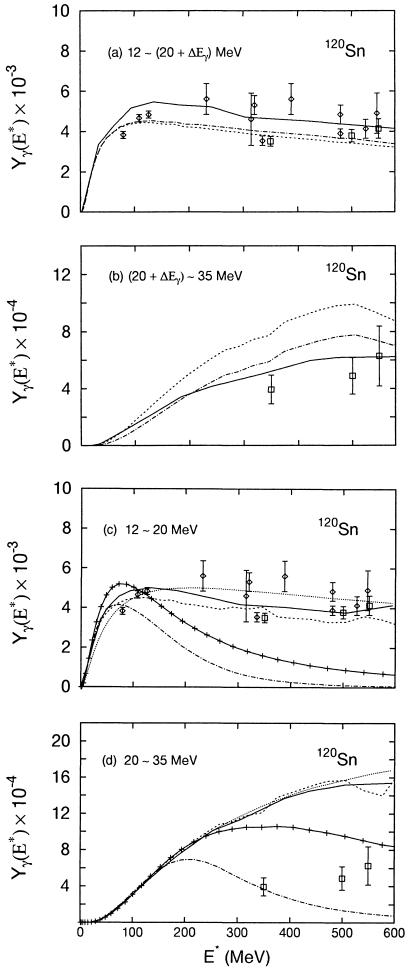

Fig. 9. Integrated yields of the γ rays as a function of excitation energy E^* in ^{120}Sn. Diamonds and squares: data from Refs. 9 and 10, respectively ($\Delta E_\gamma = 0$). In (a) and (b): dashed and dash-dotted: the results obtained within PDM-1 with $\Delta E_\gamma = 1$ and 2 MeV, respectively; solid: results obtained within PDM-2 with $\Delta E_\gamma = 0$. In (c) and (d): the results from the calculations using a Breit-Wigner strength function of an ω-independent width Γ_{GDR} centered at ω_{GDR} from different models are shown. Here: dashed and solid: results obtained within PDM-1 and PDM-2, respectively; dotted: results using the width from the Milan model of Ref. 14; dash-dotted and solid with crosses: results using the parametrizations of the Catania model in Refs. 16 and 17, respectively.

tribution of the GDR is rather flat in the tail above 20 MeV. As seen in Fig. 9 (b) an increase of ΔE_γ from 2 MeV to 3 MeV reduced noticeably the saturated value of the integrated yield in the region above the GDR. We emphasize that the microscopic structure of the strength function $S_q^{(i)}(\omega)$ with an ω-depedent damping $\gamma_q^{(i)}(\omega)$ is decisively important for an adequate description of both the shape as well as the integrated yield. As shown in Fig. 9 (c) and (d) a Breit-Wigner distribution with a width equal to $\Gamma_{GDR}^{(i)}$ and centered at ω_{GDR} can describe the integrated yield within the GDR region (Fig. 9 (c)) but strongly overestimates it in the region above 20 MeV (Fig. 9 (d)). Using the FWHM from the Milan model[14] leads to a similar behavior as shown by the dotted curves in Fig. 9 (c) and (d). Both the parametrizations for the width proposed in the Catania model[16,17] cannot account for the data of the yields in the GDR region as well as in the region above it as shown by the dash-dotted curves and the curves with crosses. Finally, as a prediction of our model we plot in Fig. 10 the integrated yield of γ rays calculated in

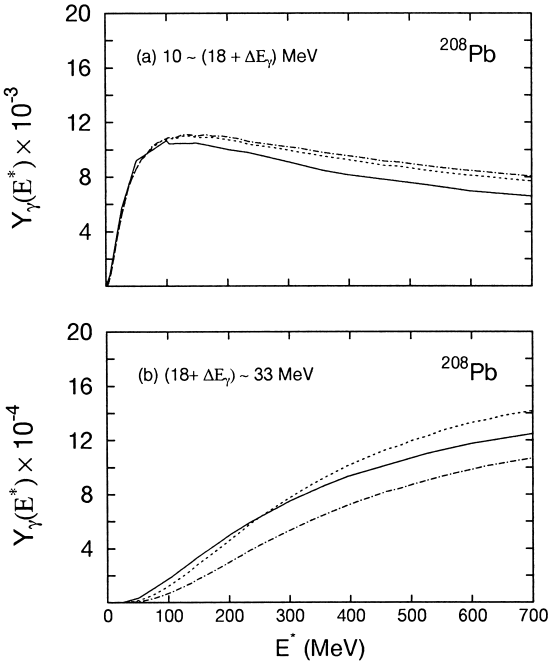

Fig. 10. Integrated yield of the γ rays as a function of excitation energy E^* in ^{208}Pb in the GDR region (a) and in the region above it (b). Notations are the same as in Fig. 9 (a) and (b).

the PDM1 and PDM2 within the interval (10–18) MeV and (18–33) MeV for ^{208}Pb. The saturated values of the yield within these intervals amount to around 8×10^{-3} and 1.2×10^{-3}, respectively.

The present calculations did not include the effects of evaporation width[28] and the GDR equilibration time[29] on the damping of the hot GDR. There are several evidents that these effects are small even at high temperatures. Indeed, it has been shown in Ref. 28 that the GDR width should reach a value of around 30 MeV due to the increase of evaporation width at $E^* = 400$ MeV. However, the same reference has also pointed out that, in order to fit the data, one needs to introduce an explicit suppression of the GDR strength when the compound nucleus reaches an excitation energy around 300 MeV. In such a case, the question of the GDR width may become irrelevant above the excitation energy where its strength vanishes or becomes too small. Existing data so far indicate a saturation, rather than an increase, of the GDR width at $E^* > 250$ MeV in good agreement with the results of our calculations. The authors of Ref. 13 have also calculated the strength function of the hot GDR including the evaporation width. They found that the overall spectra resulting from a complete CASCADE calculations are essentially identical to the ones obtained without the evaporation width even for $E^* > 120$ MeV. The contribution of the evaporation width to the total spectrum has been found to be small relatively to the total spectrum including all decay steps. The authors of Ref. 29 proposed to take into account the equilibration time of the GDR, assuming that no GDR is present at the time of formation of the compound nucleus. However, Ref. 10 has pointed out that such a hypothesis is probably reasonable if the projectile and target have the same N/Z ratio. Meanwhile, in Ref. 10, where the saturation of the integrated yield of γ rays has been reported within and above the GDR regions, the N/Z ratios of the two partners are quite different

and a substantial dipole moment is present in the entrance channel. This indicates the presence of GDR already before the equilibration is achieved. More experimental evidents are also needed to confirm whether the effects of evaporation width and equilibration time on the GDR are really small at high T.

Conclusions

The present talk gives a review of two versions PDM-1 and PDM-2 of the Phonon Damping Model (PDM) and its application to a systematic description of three main characteristics of the hot GDR, namely the GDR width, its shape and the integrated yield of γ rays, simultaneously. The results of calculations have been compared with the most recent experimental systematics assessed for these characteristics in ^{120}Sn and ^{208}Pb in the heavy-ion fusion and inelastic α-scattering reactions. An overall agreement between theory and experiment has been consistently achieved for all three characteristics.

The analysis in the present paper allows us to draw the following conclusions.
(1) This is the first time that theory gives a consistent description of the rapid increase of the width at low T as well as its saturation at $T \geq 4$ MeV taking into account the coupling of the GDR to pp and hh configurations at $T \neq 0$. Both the PDM1 and PDM2 have confirmed that the quantal width Γ_Q of the GDR due to coupling to only ph configurations decreases slightly as T increases. It becomes independent of T only when the contribution of two-phonon processes in the expansion to higher-order propagators is neglected.
(2) The PDM is a simple microscopic model yet able to reproduce reasonably well the measured shape of the GDR including some details of its fine structure.
(3) Based on the simplifying assumption of the statistical model the PDM provides a reasonable account for the experimental integrated yield of γ rays using the microscopically calculated width of the GDR. Our model describes well the saturation of the yield in both regions of the GDR and above it, showing a well defined GDR shape up to $T \sim 6$ MeV. This indicates the existence of the hot GDR even at rather high temperatures, provided that the energy-weighted sum rule value is well conserved.
(4) The present versions of the PDM did not yet include a number of effects discussed in the literature, e.g. coupling to continuum, the temperature dependence of single-particle energies, the evaporation width, the GDR equilibration time, the dependence on angular momentum, etc. There have been several references showing that these effects may not be significant at least up to $T \sim 3$ MeV in nuclei with mass number $A \geq 120$.[7,10,11,13,19,30] The agreement between the results of PDM and the data discussed in the present paper may also serve as an indirect indication that the total contribution of these effects may not significantly alter the obtained results up to $T \sim$ 5–6 MeV.

Numerical calculations were carried out by a 64-bit Alpha AXP work-station running Digital UNIX (OSF/1) at the Computer Center of RIKEN.

References

1) K. Snover: Annu. Rev. Nucl. Part. Sci. **36**, 545 (1986); J. J. Gaardhøje: Annu. Rev. Nucl. Part. Sci. **42**, 483 (1992).
2) J. J. Gaardhøje et al.: Phys. Rev. Lett. **53**, 148 (1984); Phys. Rev. Lett. **56**, 1783 (1986).
3) D. R. Chakrabarty et al.: Phys. Rev. C **36**, 1886 (1987).
4) A. Bracco et al.: Phys. Rev. Lett. **74**, 3748 (1995).
5) M. Matiuzzi et al.: Nucl. Phys. A **612**, 262 (1997).
6) D. Pierroutsakou et al.: Nucl. Phys. A **600**, 131 (1996).
7) G. Enders et al.: Phys. Rev. Lett. **69**, 249 (1992).
8) H. J. Hofmann et al.: Nucl. Phys. A **571**, 301 (1994).
9) K. Yoshida et al.: Phys. Lett. B **245**, 7 (1990); J. Kasagi et al.: Nucl. Phys. A **538**, 585c (1992); J. Kasagi and K. Yoshida: Nucl. Phys. A **557**, 221c (1993).
10) P. Piattelli et al.: Nucl. Phys. A **599**, 63c (1996); T. Suomijärvi et al.: Phys. Rev. C **53**, 2258 (1996).
11) K. Sugawara-Tanabe and K. Tanabe: Prog. Theor. Phys. **76**, 1272 (1986).
12) E. Ramakrishnan et al.: Phys. Rev. Lett. **76**, 2025 (1996); Phys. Lett. B **383**, 252 (1996).
13) T. Baumann et al.: Nucl. Phys. A **635**, 428 (1998).
14) R. A. Broglia, B. F. Bortignon, and A. Bracco: Prog. Part. Nucl. Phys. **28**, 517 (1992).
15) W. E. Ormand, P. F. Bortignon, and R. A. Broglia: Phys. Rev. Lett. **77**, 607 (1996); W. E. Ormand et al.: Nucl. Phys. A **614**, 217 (1997).
16) P. Chomaz, M. Di Toro, and A. Smerzi: Nucl. Phys. A **563**, 509 (1993).
17) A. Bonasera, M. Di Toro, A. Smerzi, and D. M. Brink: Nucl. Phys. A **569**, 215c (1994).
18) V. Baran et al.: Nucl. Phys. A **599**, 29c (1996).
19) G. Gervais, M. Thoennessen, and W. E. Ormand: Phys. Rev. C **58**, 1377R (1998).
20) N. Dinh Dang and A. Arima: Phys. Rev. Lett. **80**, 4145 (1998); Nucl. Phys. A **636**, 427 (1998).
21) N. Dinh Dang, K. Tanabe, and A. Arima: Phys. Lett. B **445**, 1 (1998); Phys. Rev. C **58**, 3374 (1998); Nucl. Phys. A **645**, 536 (1999).
22) N. N. Bogolyubov and S. Tyablikov: Sov. Phys. Doklady **4**, 6 (1959).
23) D. N. Zubarev: *Nonequilibrium Statistical Thermodynamics* (Plenum, New York, 1974); Sov. Phys. Uspekhi **3**, 320 (1960).
24) P. F. Bortignon et al.: Nucl. Phys. A **460**, 149 (1986).
25) N. Dinh Dang: Nucl. Phys. A **504**, 143 (1989).
26) J. E. Draper et al.: Phys. Rev. Lett. **49**, 434 (1982).
27) V. Zelevinsky et al.: Phys. Rep. **276**, 85 (1996).
28) Ph. Chomaz: Phys. Lett. B **347**, 1 (1995);
29) P. F. Bortignon et al.: Phys. Rev. Lett. **67**, 3360 (1991).
30) H. Sagawa and G. F. Bertsch: Phys. Lett. B **146**, 138 (1984).